Available online at www.sciencedirect.com
ScienceDirect
Ceramics International 35 (2009) 1115–1120
CERAMICS INTERNATIONAL
www.elsevier.com/locate/ceramint

Densification and grain growth during solid state sintering of $LaPO_4$

Damien Bregiroux [a,*], Fabienne Audubert [b], Didier Bernache-Assollant [c]

[a] *Universite Pierre et Marie Curie—Paris 06, CNRS UMR 7574, Chimie de la Matière Condensée de Paris, 4 Place Jussieu, F-75252 Paris Cedex 05, France*
[b] *Commissariat à l'Énergie Atomique, DEN/DEC/SPUA, Cadarache, F-13108 Saint Paul Lez Durance, France*
[c] *École Nationale Supérieure des Mines, CIS, F-42023 Saint Etienne, France*

Received 25 March 2008; received in revised form 9 April 2008; accepted 12 May 2008
Available online 19 July 2008

Abstract

This work is devoted to the kinetic study of densification and grain growth of $LaPO_4$ ceramics. By sintering at a temperature close to 1500 °C, densification rate can reach up to 98% of the theoretical density and grain growth can be controlled in the range 0.6–4 μm. Isothermal shrinkage measurements carried out by dilatometry revealed that densification occurs by lattice diffusion from the grain boundary to the neck. The activation energy for densification (E_D) is evaluated as 480 ± 4 kJ mol^{-1}. Grain growth is governed by lattice diffusion controlled pore drag and the activation energy (E_G) is found to be 603 ± 2 kJ mol^{-1}. The pore mobility is so low that grain growth only occurs for almost fully dense materials.

Keywords: A. Sintering; A. Grain growth; B. Grain size; B. Microstructure-final

1. Introduction

Lanthanum orthophosphate, a synthetic form of monazite, is a promising material for various applications. Extensive studies have been carried out in the frame of researches related to the specific conditioning of long life radionuclides in dedicated phosphate ceramics [1–5], highlighting strong resistance to aqueous alteration [6–9], and to radiation damage [10–14]. Monazite is also an attractive material for interlayers in oxide/oxide composites since it is stable with the majority of structural oxides, and makes weak bonds with them, providing efficient crack deflections [15,16]. Sr-doped $LaPO_4$ is used as solid state high temperature protonic conductors in hydrogen fuel cells [17,18]. Finally, when doped with Ce^{3+} and Tb^{3+}, $LaPO_4$ is an efficient green component of trichromatic lamp phosphors [19,20].

Powders with monazite crystal structure can be obtained by several chemical processes, involving wet or solid state routes [21,22]. Thanks to the lot of works carried out in this field since several decades, it is now well known how to control the grain size and shape [23], as well as the homogeneity of solid solutions [24]. Nevertheless, all the above applications will require production of ceramics with controlled density and microstructure. Thus, sintering, which determines end-product microstructure, is therefore an essential step for the control and optimization of the properties sought in the finished product [25].

The first works dealing with sintering of monazite-type powders were performed by Hikichi et al. in 1990s [26–28]. He showed that a monazite powder with a specific surface area close to 70 m^2 g^{-1}, synthesized through a liquid route, can be densified up to 95% of the theoretical density at 1150 °C for 3 h, whereas a 1 m^2 g^{-1} powder, synthesized by high temperature solid–solid reaction, do not sinter, even at 1600 °C. More recently, Zhifeng et al. obtained 95% dense pellets of $CePO_4$ by sintering at 1500 °C for 1 h [29]. But he did not give any information about the starting powder characteristics. Starting with nanoparticles of $EuPO_4$, Hernándes and Martín obtained sintered bodies with a relative density over 98% of the theoretical density [30]. The grains are ranged between 2 and 30 μm, according to the sintering temperature. In a previous paper, we showed how few percents of $La(PO_3)_3$ in $LaPO_4$, prepared by precipitation, modify considerably the sintering behavior by accelerating the densification but also by activating fast grain growth [31].

* Corresponding author. Tel.: +33 144274770; fax: +33 144272548.
E-mail address: damien.bregiroux@upmc.fr (D. Bregiroux).

0272-8842/$34.00
doi:10.1016/j.ceramint.2008.05.005

The goal of this paper is to provide an understanding of the solid state sintering process of pure $LaPO_4$, based on the results of a kinetic study of densification and grain growth. Experimental results are modeled with a basic sintering theory assuming a monosized spherical powder.

2. Experimental

The $LaPO_4$ powder was synthesized by high temperature solid state reaction of a lanthanum oxide/$NH_4H_2PO_4$ mixture, according to the experimental protocol described elsewhere [22]. The purity of the synthesized $LaPO_4$ was checked by XRD (Bruker D8, Germany) and ^{31}P-NRM (Bruker Avance 500 Wide Bore spectrometer, Germany). The raw powder exhibited a specific surface area less than 1 $m^2\ g^{-1}$. Attrition ground powder was obtained by grinding for 4 h in water, 100 g of $LaPO_4$ powder in a 750-cm^3 teflon jar with 1 kg of a 50/50 mixture of 1 and 2 mm zirconia balls (Union Process, model 01 CE, Akron, OH, USA). The blades revolution speed was 450 rpm. The specific surface area of the ground powder was measured according to the BET method into N_2 (Micromeritics, Gemini, USA) and was found to be closed to 25 $m^2\ g^{-1}$. SEM observations revealed that the powder mainly consists on submicronic spherical particles.

Attrition ground powders was then uniaxially pressed using a pressure of 65 MPa into pellets of 10 mm in diameter without any additive. The green density of samples, determined by geometrical measurements, is close to 50% of the theoretical one. Increasing the uniaxial pressure in order to reach higher green densities provokes interfacial cracks between density regions in the green body, which enlarge during sintering. All the pellets were sintered in air. Bulk density of the sintered pieces was determined by the Archimedes method in water. The relative density of each monazite specimen was calculated as the quotient of bulk density to theoretical density (d_{th} = 5.081) [22]. Linear shrinkage was followed in air up to 1600 °C through a vertical dilatometer (Setaram TMA 92, France). Microstructures of sintered pellets were observed upon thermally etched samples SEM micrographs according to the equivalent diameter disk method using a commercial software (AnalySIS, Soft Imaging System, Olympus). For each sample, three micrographs with approximately 400 grains in each were analyzed, so that results were deduced from the treatment of more than 1000 particles.

3. Results and discussion

3.1. Densification behavior

The first step of the present work consists in following the behavior of powder compacts during the initial stage of sintering. A fall of surface area without shrinkage is observed below 800 °C (Fig. 1*a*), due to growth of interparticle necks (no grain growth occurs at such low temperatures, as shown in following sections). Note that the surface area was measured at room temperature after a thermal treatment at the considered temperature T for 5 min with an heating rate of 10 K min^{-1}. The densification mechanisms are activated when temperature

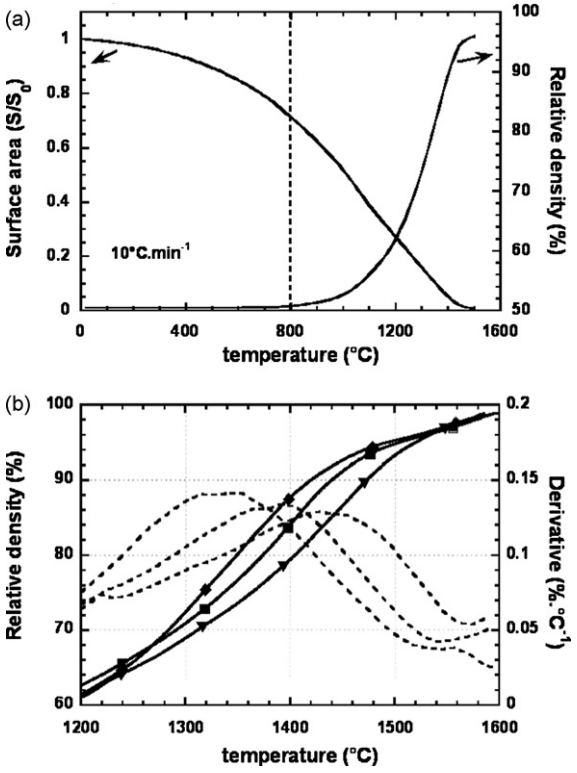

Fig. 1. Evolution with respect to the temperature of the powder surface area (S_0 = 25 $m^2\ g^{-1}$) and the pellets relative density (*a*) and for various heating rate (*b*) with ◆: 3 °C min^{-1}, ■: 10 °C min^{-1} and ▼: 30 °C min^{-1}, derivative curves in dotted lines.

is increased beyond 800 °C, leading to the shrinkage of the $LaPO_4$ specimen. The maximum densification rate is found to be in the range 1400–1500 °C. Heating rate influences neither the initial temperature of shrinkage nor the final relative density (Fig. 1*b*). Nevertheless, a shift of the densification curve toward high temperatures is observed when increasing heating rate. This tendency is generally observed when grain growth is negligible during heating [32], since densification kinetic is directly linked to grain size [33]. Indeed, at lower heating rate, the $LaPO_4$ pellet stays for a longer time at a given temperature and shrinks more before reaching higher temperature.

For initial stage sintering, mass transport mechanisms are generally deduced from the two-particle model, assuming spherical particles of same size [33–35]. Based on the models of Kucsynski [36], then those of Johnson and Clarke [37,38], relative shrinkage under isothermal conditions, controlled by one diffusion step, can thus be expressed as:

For volume diffusion from the grain boundary:

$$\frac{\mathrm{d}(\Delta l/l_0)}{\mathrm{d}t} = n\left(\frac{5.34\gamma\Omega D_V}{kTG^3}\right)^n t^{n-1} \quad (1)$$

where n = 0.49.

For grain-boundary diffusion:

$$\frac{\mathrm{d}(\Delta l/l_0)}{\mathrm{d}t} = n\left(\frac{2.14\gamma\Omega b D_B}{kTG^4}\right)^n t^{n-1} \quad (2)$$

where n = 0.33.

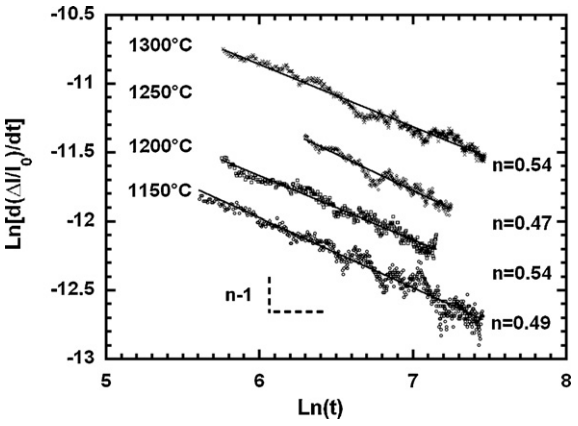

Fig. 2. Ln(d(Δl/l_0)/dt) versus ln(t) for pellets of attrition-milled $LaPO_4$ powder sintered in air.

In Eqs. (1) and (2), γ is the surface tension (assuming to be isotropic), Ω is the atomic volume, D_V and D_B are the volume and grain-boundary diffusion coefficients, respectively, k is the Boltzmann constant, T is the temperature, expressed in Kelvin, G is the particle radius and b is the thickness of the grain boundary. The mass transport mechanism for densification during the initial stage of sintering is deduced from the knowledge of the exponent n. This could be obtained from dilatometric measurements carried out under isothermal conditions. The slop of the plot of ln(d(Δl/l_0)/dt) versus ln(t) is thus ($n-1$). For the attrition-milled $LaPO_4$ powder, n is found to be close to 0.5 (±0.04) for the four temperatures tested (Fig. 2), suggesting the rate controlling mechanism for densification to be lattice diffusion from the grain boundary to the neck.

The variations of the relative density as a function of time during the intermediate and final stages of sintering are plotted in Fig. 3*a*. The mathematical relation used to fit the densification curves is:

$$\rho = \rho_0 + A(1 - e^{-bt}) \quad (3)$$

where ρ_0 is the initial relative density (at time $t = 0$). A and b are the two constant terms. Let us emphasize that Eq. (3) is just a mathematical relation and is not deduced from a theoretical model.

A relative density close to 98% of the theoretical value can be reached by sintering at least at 1425 °C for 1 h. The activation energy for densification was estimated from an Arrhenius plot of the instantaneous densification rate at constant relative density (Fig. 3*b*), assuming a negligible grain growth (assumption checked in Section 3.2 of this paper, Fig. 6).

The activation energy for densification (E_D) is evaluated as 480 ± 4 kJ mol^{-1} from the slopes of the linear representation of Fig. 3*b*. As far as we know, this value has not been reported before this work.

3.2. Grain growth and microstructure development

Fig. 4 depicts the evolution of average grain size with time for several sintering temperatures. Note that the average grain

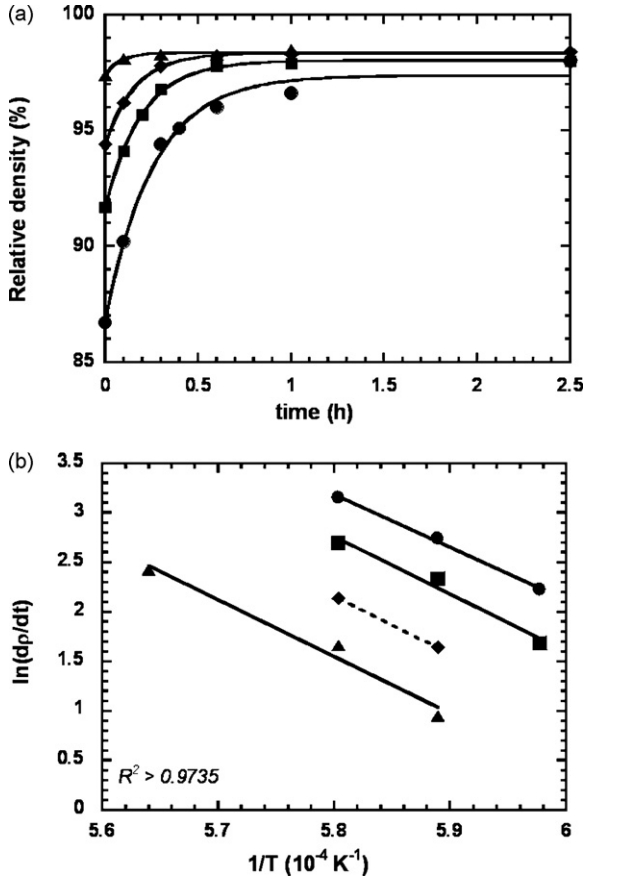

Fig. 3. Effect of the sintering temperature on the evolution of the relative density versus time for $LaPO_4$ (*a*) ●: 1400 °C, ■: 1425 °C, ◆: 1450 °C and ▲: 1500 °C and the Arrhenius plot of the densification rate at given relative densities (*b*) ●: 95%, ■: 96%, ◆: 97% and ▲: 97.5%.

size reaches 4 μm after sintering at 1500 °C for 20 h. For a clarity consideration, this point is not plotted on Fig. 4. Except for materials sintered at 1400 °C with a sintering time less than half an hour, all the pellets used for Fig. 4 present a relative density higher than 92% of the theoretical one (see Fig. 3*a*).

An example of the typical final microstructure obtained for dense $LaPO_4$ pellets is shown in Fig. 4. On all the samples observed, residual pores remain located on the grain edges (closed intergranular porosity) so that abnormal grain growth is minimized, which it is expected in the quest of high density ceramics. Grain size distribution appears to be quite homogeneous, follows a log-normal law and remains invariant when changing the sintering conditions (i.e., temperature and time) as shown in Fig. 5. This invariance is representative of a normal grain growth. The cumulative normalized grain size distribution can be modeled by the following relation:

$$\Phi(\%) = 100 \times \left[1 - \exp\left(-b\frac{G}{G_m}\right)\right] \quad (4)$$

where b is close to 0.8, in good accordance with the observations of German made on several liquid-phase sintered materials ($b \approx 0.7$) [34]. This observation is also valid for powders milled under different conditions. It is worth to note that the

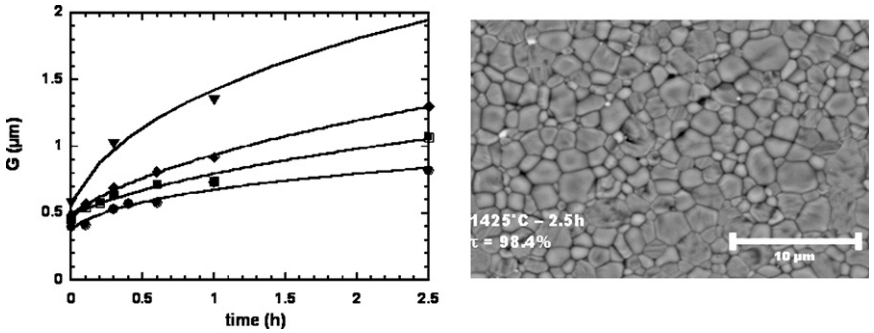

Fig. 4. Effect of temperature on the grain growth kinetic of sintered $LaPO_4$ pellets (●: 1400 °C, ■: 1425 °C, ◆: 1450 °C and ▼: 1500 °C) and typical resulting microstructure.

final grain size distribution is similar for all samples, whatever the initial particle size distribution.

The above observations reveal that the porosity only consists on closed porosity (relative density higher than 92% of the theoretical one). Normal grain growth occurs because this closed porosity remains located on the grain boundary. The grain growth kinetic is therefore governed by the grain boundary mobility (grain boundary control) or by the pore one (pore control) [39].

In the present work, the role of porosity located on grain boundaries on the microstructure development of $LaPO_4$ is clearly shown on the sintering path of Fig. 6. Up to 97.5% of the theoretical density, grain growth appears to be negligible, which confirms the assumption made previously for the determination of the activation energy for densification. Above 97.5%, mean grain size can be increased at least by a factor of 6, i.e., from 0.6 to 4 μm. At such high densities, the few pores remaining on the grain boundaries have a sufficiently low size so that their mobility becomes close to that of grain boundary. Thereby, grain growth rate is considerably enhanced. This is clearly illustrated by the micrograph of Fig. 6: large grains are observed in the dense zone, in the center, whereas in the porous zones, on the edges of the micrograph, the grains remain small. This is clearly indicative of a pore control grain growth.

Thanks to these observations, experimental results can be thus modeled assuming a normal grain growth in a nearly fully dense material, through the following kinetic equation [40]:

$$G^m - G_0^m = k(T)t \tag{5}$$

where

$$k(T) = \frac{k_0}{T} e^{-E_G/RT} \tag{6}$$

In Eqs. (5) and (6), G is the grain size ($G = G_0$ at time $t = 0$), m is a constant representative of the grain growth mechanism, k is the kinetic constant, inversely proportional to the temperature T, k_0 is the pre-exponential term, R is the universal gas constant and E_G is the activation energy of the process controlling grain growth.

The data of Fig. 4 were fitted with the function of Eq. (5). The resulting parameters are given in Table 1. The growth exponent m is in the range 2.6–2.8, except at 1400 °C. Nevertheless, it is important to remind that the used grain growth model is valid only for microstructure without open porosity, which is not the case at 1400 °C [40].

The fitting of our experimental data lead to a m value lying in the range 2–3. The interpretation of these results should be done very carefully. Indeed, in the general equation $G^m - G_0^m = k(T)t$, m should be a whole number according to the grain growth mechanism involved. But insofar that many approximations have been done in this model, i.e., homogeneous compact, spherical pores, isotropic grain boundary energy, etc., the experimental value of m is generally not integer. Furthermore,

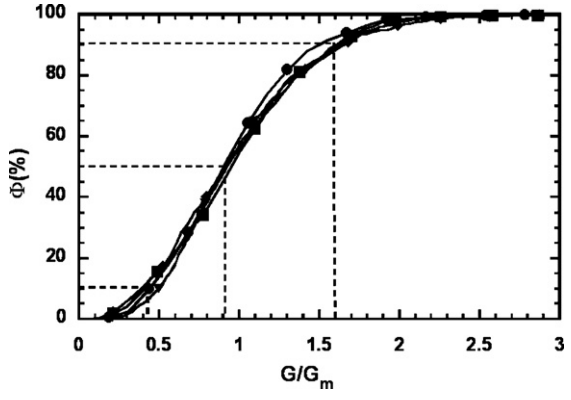

Fig. 5. Self-similarity of cumulative grain size distribution of $LaPO_4$ pellets for various sintering conditions (●: 1400 °C—0 h, ■: 1425 °C—2.5 h, ◆: 1450 °C—2.5 h and ▼: 1500 °C—20 h). The grain size axis is normalized to the mean grain size G_m.

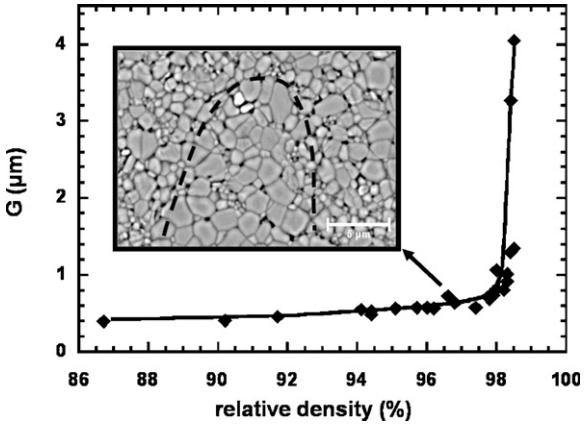

Fig. 6. Grain size/density trajectory for $LaPO_4$ sintered in air.

Table 1
Grain growth parameters for sintered $LaPO_4$ pellets obtained from the fitting of the experimental results with the kinetic law $G^m - G_0^m = k(T)t$

Temperature (°C)	G_0 (μm)	k ($\mu m^m\ s^{-1}$)	m	R^2
1400	0.38 ± 0.04	0.19 ± 0.05	4.0 ± 0.8	0.9605
1425	0.49 ± 0.03	0.40 ± 0.05	2.6 ± 0.7	0.9745
1450	0.50 ± 0.01	0.68 ± 0.04	2.6 ± 0.2	0.9983
1500	0.58 ± 0.08	2.40 ± 0.50	2.8 ± 0.2	0.9983

simultaneous mechanisms could occur during the microstructure development. Nevertheless, assuming a pore control of the microstructure development in a pure system, as demonstrated previously, three possible grain growth mechanisms could occur:

(i) Pore displacement controlled by surface diffusion ($m = 4$).
(ii) Pore displacement controlled by lattice diffusion ($m = 3$).
(iii) Pore displacement controlled by vapor transport ($m = 2$ or 3).

Considering that $LaPO_4$ is a very refractory material with a melting point higher than 2000 °C, coarsening by vapor diffusion is very dubious. Consequently, it is reasonable to conclude that data are best adjusted with a value of $m = 3$, indicative of a pore displacement controlled by lattice diffusion process.

The determination of the activation energy E_G could be obtained by the derivative of Eq. (5):

$$\frac{dG}{dt} = \frac{k_0}{mT} e^{-E_G/RT} G^{(1-m)/m} \quad (7)$$

The activation energy is thus deduced from the slope of the plot $\ln(T(dG/dt) = f(1/T))$ at a given grain size G:

$$\ln\left(T\frac{dG}{dt}\right)_G = -\frac{E_G}{R}\frac{1}{T} + \ln\left(\frac{k_0}{m}G^{(1-m)/m}\right) \quad (8)$$

The activation energy is evaluated as 603 ± 2 kJ mol^{-1} and is constant, whatever the grain size (Fig. 7). The invariance of both m and E_G is a strong argument making possible to claim that the transport mechanism remains unchanged during grain growth.

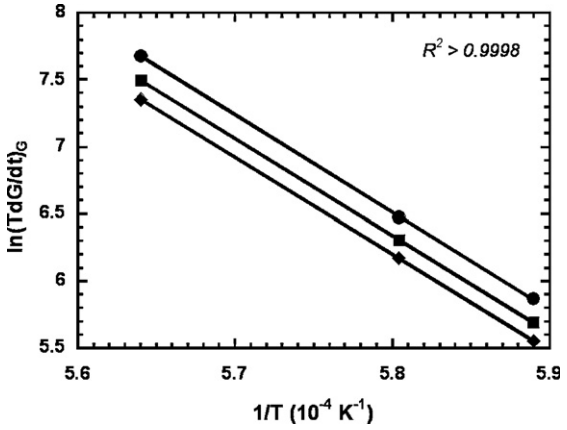

Fig. 7. Arrhenius plot of the grain growth rate $\ln(T(dG/dt)/dt)_G$ for given grain size G (●: 0.6 μm, ■: 0.8 μm and ◆: 1 μm).

We found that the activation energy of grain growth is higher than that of densification. The consequence is that densification is predominant at low temperature. Such an unusual result has already been observed for MgO [41]. Thus a low heating rate allows to reach high densities before grain growth mechanism is activated. As we showed in this paper, grain growth only occurs when porosity located at grain boundaries is negligible, i.e., for very high densities. Moreover, the lower heating rate is, the higher the sintering time. Consequently, for a given sintering temperature, a slow heating rate enhances grain growth. This was experimentally observed. The analysis of the resulting microstructure of the three pellets used for the dilatometric measurements presented in Fig. 1 revealed that the final grain size is linked to the heating rate. For heating rates of 1, 10 and 30 °C min^{-1}, the final mean grain size after sintering at 1600 °C for 1 min is 2.6, 1.8 and 2.0 μm, respectively. Large grains are obtained with very low heating rate.

4. Conclusions

The sintering of $LaPO_4$ was investigated on an attrition milled powder with a specific surface area of 25 $m^2\ g^{-1}$. Densification starts at 800 °C and the optimum sintering temperature is in the range 1450–1500 °C. Without any additives or additional external pressure, it is possible to obtain ceramics with densification rate close to 98% of the theoretical density. Grain growth can be controlled in the range 0.6–4 μm. It as been shown that densification occurs by lattice diffusion from the grain boundary to the neck. Grain growth is governed by lattice diffusion controlled pore drag. The porosity located at the grain boundaries inhibits grain growth. It is therefore essential to reach very high density in order to make the grains grow. This could be achieved by sintering with a slow heating rate.

Next studies will involve the investigation of the relationship between microstructure and properties, as we already done for mechanical and thermal properties [25].

Acknowledgements

Based in part on the thesis submitted by D. Bregiroux, Université de Limoges, France, 2005, this work was financially and scientifically supported by the French Research Group NOMADE (GdR 2023, CNRS/CEA/COGEMA) and by a CEA-CFR research grant.

References

[1] D. Bregiroux, F. Audubert, E. Champion, D. Bernache-Assollant, Mechanical and thermal properties of hot pressed neodymium-substituted britholite $Ca_9Nd(PO_4)_5(SiO_4)F_2$, Mater. Lett. 57 (2003) 3526–3531.
[2] N. Dacheux, N. Clavier, A.C. Robisson, O. Terra, F. Audubert, J.E. Lartigue, C. Guy, Immobilisation of actinides in phosphate matrices, C. R. Chim. 7 (2004) 1141–1152.
[3] N. Clavier, N. Dacheux, R. Podor, Synthesis, characterization, sintering, and leaching of β-TUPD/monazite radwaste matrices, Inorg. Chem. 45 (2006) 220–229.

[4] N. Clavier, N. Dacheux, G. Wallez, M. Quarton, Improvement of the preparation of sintered pellets of thorium phosphate–diphosphate and associated solid solutions from crystallized precursors, J. Nucl. Mater. 352 (2006) 209–216.
[5] O. Terra, N. Dacheux, F. Audubert, R. Podor, Immobilization of tetravalent actinides in phosphate ceramics, J. Nucl. Mater. 352 (2006) 224–232.
[6] O. Terra, N. Clavier, N. Dacheux, R. Podor, Preparation and characterization of lanthanum–gadolinium monazites as ceramics for radioactive waste storage, N. J. Chem. 27 (2003) 957–967.
[7] F. Poitrasson, E.H. Oelkers, J. Schott, J.M. Montel, Experimental determination of synthetic $NdPO_4$ monazite end-member solubility in water from 21 °C to 300 °C: implications for rare earth element mobility in crustal fluids, Geochim. Cosmochim. Acta 68 (2004) 2207–2221.
[8] E.H. Oelkers, F. Poitrasson, An experimental study of the dissolution stoichiometry and rates of a natural monazite as a function of temperature from 50 to 230 °C and pH from 1.5 to 10, Chem. Geol. 191 (2002) 73–87.
[9] Z.S. Cetiner, S.A. Wood, C.H. Gammons, The aqueous geochemistry of the rare earth elements. Part XIV. The solubility of rare earth element phosphates from 23 to 150 °C, Chem. Geol. 217 (2005) 147–169.
[10] R.C. Ewing, R.F. Haaker, The metamict state: implications for radiation damage in crystalline waste forms, Nucl. Chem. Waste Manage. 1 (1980) 51–57.
[11] F.G. Karioris, K. Appaji Goda, L. Cartz, Heavy ion bombardment of monoclinic $ThSiO_4$, ThO_2 and monazite, Radiat. Eff. Lett. 58 (1981) 1–3.
[12] A. Meldrum, L.A. Boatner, W.J. Weber, R.C. Ewing, Radiation damage in zircon and monazite, Geochim. Cosmochim. Acta 62 (1998) 2509–2520.
[13] B.E. Burakov, M.A. Yagovkina, M. Garbuzov, A. Kitsay, V.A. Zirlin, Self-irradiation of monazite ceramics: Contrasting behavior of $PuPO_4$ and $(La,Pu)PO_4$ doped with Pu-238, Mater. Res. Soc. Symp. Proc. 824 (2004) 219–224.
[14] D. Bregiroux, R. Belin, P. Valenza, F. Audubert, D. Bernache-Assollant, Plutonium and americium monazite materials: solid state synthesis and X-ray diffraction study, J. Nucl. Mater. 366 (2007) 52–57.
[15] J.B. Davis, D.B. Marshall, P.E.D. Morgan, Monazite-containing oxide/oxide composites, J. Eur. Ceram. Soc. 20 (2000) 583–587.
[16] P. Mogilevsky, E.E. Boakye, R.S. Hay, Solid solubility and thermal expansion in a $LaPO_4$–YPO_4 system, J. Am. Ceram. Soc. 90 (2007) 1899–1907.
[17] K. Amezawa, H. Maekawa, Y. Tomii, N. Yamamoto, Protonic conduction and defect structures in Sr-doped $LaPO_4$, Solid State Ionics 145 (2001) 233–240.
[18] N. Kitamura, K. Amezawa, Y. Uchimoto, Y. Tomii, T. Hanada, N. Yamamoto, Electrical conduction properties of rare earth orthophosphates under reducing conditions, Solid State Ionics 177 (2006) 2369–2373.
[19] M.Z. Su, J. Zhou, K.S. Shao, Reaction mechanism for the solid state synthesis of $LaPO_4$: Ce, Tb phosphor, J. Alloy Compd. 207 (1994) 406–408.
[20] C. Wu, Y. Wang, W. Jie, Hydrothermal synthesis and luminescent properties of $LnPO_4$:Tb (Ln = La, Gd) phosphors under VUV excitation, J. Alloy Compd. 436 (2007) 383–386.
[21] S. Lucas, E. Champion, D. Bregiroux, D. Bernache-Assollant, F. Audubert, Rare eath phosphate powders $RePO_4$–nH_2O (Re = La, Ce or Y). Part I. Synthesis and characterization, J. Solid State Chem. 177 (2004) 1302–1311.
[22] D. Bregiroux, F. Audubert, T. Charpentier, D. Sakellariou, D. Bernache-Assollant, Solid-state synthesis of monazite-type compounds $LnPO_4$ (Ln = La to Gd), Solid State Sci. 9 (2007) 432–439.
[23] L. Karpowich, S. Wilcke, R. Yu, G. Harley, J.A. Reimer, L.C. De Jonghe, Synthesis and characterization of mixed-morphology $CePO_4$ nanoparticles, J. Solid State Chem. 180 (2007) 840–846.
[24] D. Bregiroux, O. Terra, F. Audubert, N. Dacheux, V. Serin, R. Podor, D. Bernache-Assollant, Solid state synthesis of monazite-type compounds containing tetravalent elements, Inorg. Chem. 46 (2007) 10372–10383.
[25] L. Perrière, D. Bregiroux, B. Naïtali, F. Audubert, E. Champion, D.S. Smith, D. Bernache-Assollant, Microstructural dependence of the thermal and mechanical properties of monazite $LnPO_4$ (Ln = La to Gd), J. Eur. Ceram. Soc. 27 (2007) 3207–3213.
[26] Y. Hikichi, T. Nomura, Y. Tanimura, S. Susuki, Sintering and properties of monazite-type $CePO_4$, J. Am. Ceram. Soc. 73 (1990) 3594–3596.
[27] Y. Hikichi, T. Ota, Sintering and properties of monazite-type RPO_4 (R = La, Ce, Nd or Sm), Phosphorus Res. Bull. 6 (1996) 175–178.
[28] Y. Hikichi, T. Ota, T. Hattori, Thermal, mechanical and chemical properties of sintered monazite–(La, Ce, Nd, Sm), Miner. J. 19 (1997) 123–130.
[29] L. Zhifeng, L. Jiachen, Q. Shipeng, J. Zhengguo, Sintering and machinability of monazite-type $CePO_4$ ceramics, J. Rare Earth 21 (2003) 99–101.
[30] T. Hernándes, P. Martín, Microstructural and optical features of a Eu–monazite, J. Eur. Ceram. Soc. 27 (2007) 109–114.
[31] D. Bregiroux, S. Lucas, E. Champion, F. Audubert, D. Bernache-Assollant, Sintering and microstructure of rare earth phosphate ceramics $REPO_4$ with RE = La, Ce or Y, J. Eur. Ceram. Soc. 26 (2006) 279–287.
[32] G. Bernard-Granger, C. Guizard, Apparent activation energy for the densification of a commercially available granulated zirconia powder, J. Am. Ceram. Soc. 90 (2007) 1246–1250.
[33] S.J.L. Kang, Sintering, Densification, Grain Growth & Microstructure, Elsevier Butterworth–Heinemann, Oxford, 2005.
[34] N.J. Shaw, Densification and coarsening during solid state sintering of ceramics: a review of the models. I. Densification, Powder Metall. Int. 21 (1989) 16–21.
[35] R.M. German, Sintering Theory and Practice, John Wiley & Sons, Inc., 1996.
[36] G.C. Kuczynski, Self diffusion in sintering of metallic particles, Trans. Am. Inst. Miner. 185 (1949) 169–178.
[37] D.L. Johnson, T.M. Glarke, Grain boundary and volume diffusion in the sintering of silver, Acta Met. 12 (1964) 1173–1179.
[38] D.L. Johnson, New method of obtaining volume, grain-boundary, and surface diffusion coefficients from sintering data, J. Appl. Phys. 40 (1969) 192–200.
[39] N.J. Shaw, Densification and coarsening during solid state sintering of ceramics: a review of the models. II. Grain growth, Powder Metall. Int. 21 (1989) 31–33.
[40] R.J. Brook, in: F.F.Y. Wang (Ed.), Controlled Grain Growth, Academic Press, New York, 1976.
[41] C.A. Handwerker, R.M. Cannon, R.L. Cannon, Final-stage densification of MgO, Structure and Properties of MgO and Al_2O_3 Ceramics, vol. 10, The American Ceramic Society, Columbus, OH, 1983, pp. 619–643.